This is the accepted manuscript made available via CHORUS. The article has been published as:

Ab initio elasticity at finite temperature and stress in ferroelectrics

Mark A. Mathis and Chris A. Marianetti

Phys. Rev. B **110**, L140101 — Published 3 October 2024

DOI: 10.1103/PhysRevB.110.L140101

Ab initio elasticity at finite temperature and stress in ferroelectrics

Mark A. Mathis and Chris A. Marianetti
Department of Applied Physics and Applied Mathematics, Columbia University, New York, NY 10027

Computing the temperature and stress dependence of the elastic constants from first-principles in non-cubic materials remains a challenging problem. Here we circumvent the aforementioned challenge via the generalized quasiharmonic approximation (gQHA) with the irreducible derivative approach for computing strain dependent phonons using finite difference, explicitly including dipole-quadrupole contributions. We showcase the gQHA in ferroelectric $PbTiO_3$, computing all elastic constants and piezoelectric strain coefficients at finite temperature and stress. The gQHA overestimates the temperature dependence of the lattice parameters and elastic constant tensor, demonstrating the need for an explicit treatment of lattice anharmonicity as a function of strain.

Ferroelectric materials have been widely studied due to technological importance and interesting physics [1–5]. Many ferroelectric materials are band insulators, which are typically well described by density functional theory (DFT) when using an appropriate exchange-correlation functional. Various studies of ferroelectrics which parametrize an interacting phonon Hamiltonian based on DFT and solve the Hamiltonian within quantum Monte-Carlo have produced temperature dependent structural phase transitions consistent with experiment [6–9]. However, evaluating piezoelectric properties at finite temperatures and stress requires the computation of relevant strain curvatures of the DFT based vibrational free energy at finite temperatures and stress (i.e. the elastic constants). Computing these elastic constants requires encoding or sampling the vibrational Hamiltonian as a function of strain, evaluating the vibrational free energy in some approximation as a function of strain, and evaluating the second strain derivatives of the free energy. Each of the aforementioned tasks presents substantial theoretical and computational challenges.

The standard approximation for computing finite temperature elastic constants is the quasiharmonic approximation (QHA) [10–13], yielding reasonable agreement with experimental measurements for a variety of cubic systems [14–21]. The computational cost of executing the QHA within DFT is appreciable [22], as evidenced by the sparsity of temperature dependent elastic constant computations for non-cubic systems available in the literature [23–25], and we are not aware of any published results at finite temperature and anisotropic stress. The aforementioned limitations can be mitigated by using the recently developed generalized quasiharmonic approximation (gQHA) [26], which leverages the irreducible derivative approach to computing phonons [27, 28]. We define the gQHA as a harmonic truncation of the Born-Oppenheimer potential at a given strain, where no additional approximations are made when evaluating the free energy or any other thermal averages. Here we showcase the power of the gQHA by studying the displacive ferroelectric $PbTiO_3$ (space group P4mm) using DFT, computing the lattice parameters, full elastic constant tensor, and piezoelectric strain coefficients at finite temperature and stress. $PbTiO_3$ is an ideal candidate to study within the gQHA, as the low symmetry ferroelectric phase persists to approximately $T = 760$ K [29–31].

Method	a	c	z(Ti)	z(O_1)	z($O_{2,3}$)
PBEsol (DFT)	3.872	4.214	0.539	0.118	0.623
SCAN (DFT)	3.865	4.341	0.545	0.139	0.638
PBEsol (gQHA)	3.891	4.164	0.539	0.112	0.618
Mestric et al.	3.891	4.168	0.542	0.124	0.629

TABLE I. Lattice parameters and direct atomic coordinates along the z-direction. (Top) Results of DFT relaxation using the PBEsol and SCAN functionals. (Bottom) Results from the gQHA at $T = 1$ K compared with experimental measurements at $T = 12$ K [41].

DFT calculations were performed using the Vienna *ab initio* simulation package (VASP) [32–35] with the projector augmented wave (PAW) method [36, 37] unless otherwise stated. The generalized gradient approximation (GGA) revised for solids (PBEsol) [38] and the strongly constrained and appropriately normed (SCAN) [39] exchange-correlation functionals were used. Convergence of the strain dependent phonons was achieved with a kinetic energy cutoff of 1000 eV and a Γ-centered **k**-point mesh of 16×16×16 for the primitive unit cell with corresponding mesh densities being used for supercells. Details of the PAW potentials, computations of the phonons as a function of strain, and Fourier interpolation are provided in Sec. SI of the supplemental material (SM) [40]. The Taylor series expansion of the Born-Oppenheimer potential is truncated at fifth order in mixed displacement and strain derivatives unless otherwise stated. The validity of the fifth order Taylor series expansion is confirmed up to $T = 350$ K by comparing to the thermal expansion resulting from the evaluation of the second order irreducible derivatives on a strain grid and then interpolating (see SM for additional details [40]). The relaxed crystal structures using the PBEsol and SCAN functionals are compared with low temperature experimental measurements in Table I. Due to the significant overestimation of the c lattice parameter by the SCAN functional, our computations use the PBEsol functional unless otherwise stated.

We begin by showcasing the phonons commensurate

with the $4 \times 4 \times 4$ supercell computed at the relaxed lattice parameters (see Fig. 1 (a)), achieving reasonable agreement with previous computations [42]. The Fourier interpolated phonons include the dipole-dipole contribution [26, 43, 44] shown as the red lines, where the dielectric tensor and Born effective charges were calculated from density functional perturbation theory [45, 46] within VASP. Along the path from the Γ point to the R point, there are interpolated imaginary phonon frequencies caused by a deficiency in the Fourier interpolation. Supplementing the interpolation with the dipole-quadrupole interactions has demonstrated the ability to remove these spurious imaginary frequencies from the interpolation [47]. Our Fourier interpolation of the phonons including the dipole-dipole and the dipole-quadrupole contributions shown as the blue lines does not contain any spurious imaginary frequencies. Computation of the dipole-quadrupole contribution has been implemented analogously to the dipole-dipole contribution, where dynamical quadrupoles were computed [48] using density functional theory implemented in the (ABINIT) package [49, 50] using the PBEsol optimized norm-conserving Vanderbilt pseudopotential (ONCVPSP) [51]. Our results illustrate that both dipole-dipole and dipole-quadrupole corrections to the Fourier interpolation can straightforwardly be utilized in our irreducible derivative approaches, which are based on the finite difference method (see Appendix A of Ref. [26] and SM [40] for more information).

We now present generalized Gruneisen parameters $\gamma_{i,\mathbf{q}\ell} = -\frac{1}{\omega_{\mathbf{q}\ell}} \frac{\partial \omega_{\mathbf{q}\ell}}{\partial \epsilon_i}$ computed at the relaxed lattice parameters, encapsulating the first order strain dependence of the phonons (see Fig. 1 (b) and (c)). Computation of the full elastic constant tensor within the gQHA requires the strain dependence of the phonons for all strains, whereas the thermal expansion only requires the strain dependence of phonons for strains that do not break point group symmetry (i.e. identity strains). In $PbTiO_3$, the identity strains can be defined as $\epsilon_{A_1^\square} = \frac{1}{\sqrt{2}}(\epsilon_{xx} + \epsilon_{yy})$ and $\epsilon_{A_1^\circ} = \epsilon_{zz}$, and the $\epsilon_{A_1^\circ}$ Gruneisen parameter is shown in Fig. 1b. Integration of the density of states yields averaged Gruneisen parameters of $\bar{\gamma}_{A_1^\square}$=1.78 and $\bar{\gamma}_{A_1^\circ}$=0.28. The Gruneisen parameter of the non-identity strain $\epsilon_{B_1} = \frac{1}{\sqrt{2}}(\epsilon_{xx} - \epsilon_{yy})$ is shown in Fig. 1c. Symmetry selection rules and first order perturbation theory require non-identity strain Gruneisen parameters to be zero along various directions in reciprocal space [26].

Having computed the strain dependence of the phonons, we apply the gQHA to compute the a and c lattice parameters at finite temperature and stress. The lattice parameters at a given temperature T and stress $\boldsymbol{\sigma}$ are computed by evaluating the Biot strain map $\tilde{\boldsymbol{\epsilon}}(T, \boldsymbol{\sigma})$, where definitions and notation are equivalent to Ref. [26] (see Eqs. 21-26). The crystal structure predicted at $T = 1$ K by the gQHA quantitatively differs from the values obtained from DFT relaxations due to zero point motion, and are compared with experimental measurements

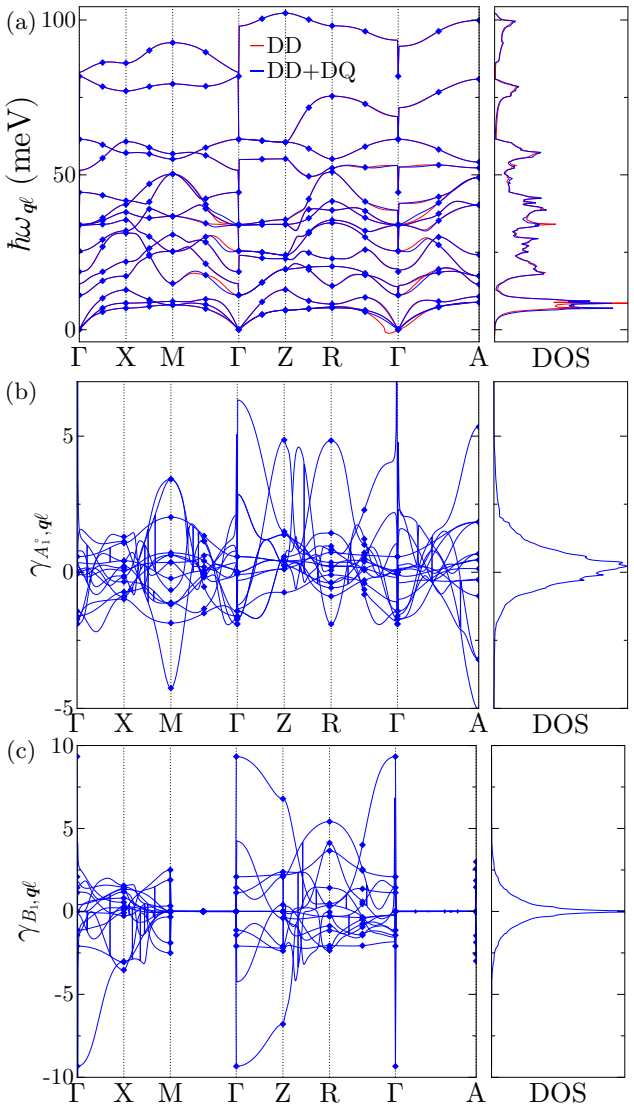


FIG. 1. Phonons and specific Gruneisen parameters computed from DFT (diamonds) and Fourier interpolated (lines), in addition to the corresponding density of states. (a) Computed phonons which are Fourier interpolated with dipole-dipole (red) or dipole-dipole and dipole-quadrupole (blue) contributions. (b, c) Gruneisen parameters corresponding to strains $\epsilon_{A_1^\circ}$ and ϵ_{B_1}, respectively.

at $T = 12$ K (see Table I). The predicted shift in lattice parameters due to zero-point motion yields remarkable agreement with the values obtained from experiment, however there are small discrepancies in the predicted basis atom positions for the oxygen atoms. It should be noted that within the gQHA, the Born-Oppenheimer potential is parametrized under the condition where the basis atom positions are always at a minimum energy. Furthermore, the Born-Oppenheimer potential is truncated at second order at a given strain, and therefore the basis atom positions are purely determined by the strain

which results from minimizing the free energy. Therefore, the gQHA yields the same result for basis atom positions as QHA methods which employ the zero-static-internal-stress approximation [52]. The calculation of basis atom positions can be improved by going beyond the QHA using the anharmonic terms (e.g. see Refs. [13] and [53–55]).

We now compare the computed temperature dependence of the lattice parameters with experimental measurements at various temperatures under unstressed conditions (see Fig. 2*a* and 2*b*). The most notable difference among the experiments is a relative shift in the a and c lattice parameters, presumably due to imperfections in the measured crystal samples. The measurements in Ref. [56] were conducted on samples with a composition including 3% and 6% Cd, and we use the room temperature measurements to linearly extrapolate to 0% Cd by shifting all measured a and c lattice parameters by 0.005 Å and -0.007 Å, respectively (shown as hollow markers). The gQHA overestimates the change in the lattice parameters with temperature, which has been observed in previous literature studying $PbTiO_3$ [42] and in various other materials [57, 58]. Given that the gQHA allows for anisotropic stress, it is interesting to apply a compressive stress of $\sigma_{A_1^{\square}} = -0.31$ GPa and a tensile stress of $\sigma_{A_1^{\circ}} = 0.055$ GPa. The applied stress shifts the a and c lattice parameters with only minor changes to the temperature dependence.

We present the change in the c lattice parameter with respect to pressure at finite temperatures in the range from $P = 0$ GPa to $P = 3$ GPa, and compare with experimental measurements at room temperature (see Fig. 2 (*c*)). The dashed black line is computed at $T = 0$ K within the classical QHA, whereby the $T = 0$ K classical result will be equivalent to the lattice parameter computed in a DFT relaxation at constant pressure, presuming that the strain dependence of the elastic energy is faithfully parametrized. The change in the lattice parameter with pressure at finite temperature is shown at temperatures of $T = 1$ K and $T = 300$ K. The computed lattice parameter at zero pressure and room temperature underestimates the measured lattice parameter [61]. There are only small differences in the pressure dependence of the lattice parameter computed at $T = 1$ K and $T = 300$ K, and the gQHA overestimates the pressure dependence of the lattice parameter as compared to the experimental measurements [61]. However, it is interesting to note that quantum fluctuations suppress the decrease of the classical gQHA result with pressure, pushing the result towards the experimental measurements.

Having computed the lattice parameters, we now discuss the strain curvature of the free energy at finite temperature and stress. There are three experimentally relevant quantities related to the free energy curvature at finite stress [62]: the free energy curvature C_{ij}, the elastic wave propagation coefficient S_{ij}, and the stress-strain coefficient B_{ij}. Additionally, elastic constants in ferroelectrics can be measured under boundary conditions of

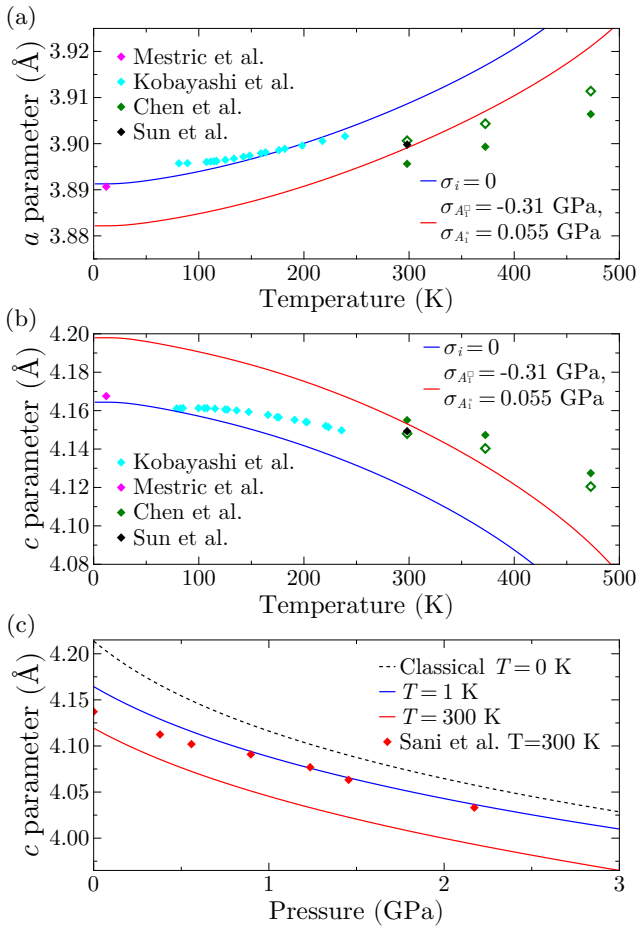


FIG. 2. The a (panel a) and c (panel b) lattice parameters as a function of temperature computed with the gQHA (lines) under unstressed (blue) and stressed (red) conditions compared with experimental measurements (diamonds) [41, 56, 59, 60]. The solid green points correspond to samples with 3% Cd, while corresponding hollow points are extrapolated to 0% Cd. (*c*) The c lattice parameter as a function of pressure computed with the gQHA at various temperatures compared with experimental measurements [61].

constant electric field E or constant electric displacement field D. The relation between the two boundary conditions is given by [63],

$$C_{ij}^{D}(T,\boldsymbol{\sigma}) = C_{ij}^{E}(T,\boldsymbol{\sigma}) + \sum_{\alpha\beta} \big(e_{\alpha i}(T,\boldsymbol{\sigma}) \times e_{\beta j}(T,\boldsymbol{\sigma})((\hat{\epsilon}^{\infty,S}(T,\boldsymbol{\sigma}))^{-1})_{\alpha\beta}\big), \quad (1)$$

where $\hat{\epsilon}^{\infty,S}$ is the relaxed-ion dielectric tensor at fixed strain and $e_{\alpha i}$ is the relaxed-ion piezoelectric stress coefficient [63–66] (see Sec. SI of SM for additional details [40]).

We compute the full elastic constant tensor at finite temperature and stress and compare with experimental values measured under unstressed conditions at room temperature and beyond [67–69] (see Fig. 3). The elas-

tic constants which were only measured at a single temperature are compared to the gQHA in Sec. SI of the SM [40]. There is reasonable agreement between the two sets of experimental values at room temperature, where the largest disagreement is a 4% difference in the measured C_{44}^D values. At room temperature, the gQHA with PBEsol yields good agreement for C_{11}^E and C_{44}^E, however C_{33}^D and C_{44}^D are overestimated and C_{66} is underestimated. The change in the predicted elastic constants with temperature is much greater than the change observed in experiment, likely due to an overestimation of the thermal expansion with temperature (see Fig. 2) and due to the neglect of explicit phonon interactions within the QHA [57, 58]. The change in the constant D-field elastic constants with temperature is significantly greater than that of the corresponding constant E-field cases, and Eq. 1 dictates that the origin is the temperature dependence of e_{ij} and $\hat{\epsilon}_{ij}^{\infty,S}$, which depend on the strain dependent Γ-point dynamical matrix. The strong temperature dependence of the constant D-field elastic constants is in stark disagreement with experiment, likely indicating a deficiency of the gQHA.

We proceed by computing the piezoelectric strain coefficients as a function of temperature and stress, and compare with existing experimental values measured under unstressed conditions (see Fig. 4 and SM [40]). The piezoelectric strain coefficients d_{ij} are constructed using the elastic constant tensor and the piezoelectric stress coefficients [63, 70],

$$d_{\alpha i}(T,\boldsymbol{\sigma}) = \sum_j ((\hat{B}^E(T,\boldsymbol{\sigma}))^{-1})_{ij} e_{\alpha j}(T,\boldsymbol{\sigma}), \qquad (2)$$

where $\hat{B}_{ij}^E$ denotes the stress-strain coefficient under a constant electric field. The graphs of d_{33} and d_{15} are shown in the SM [40] as only room temperature measurements have been performed for these coefficients. The experimentally measured values of the piezoelectric strain coefficients [68, 69, 71] show quantitative inconsistency, as the values vary as much as 20% for d_{31} at room temperature. Our quasiharmonic prediction of d_{31} overestimates the experimental measurements, and the discrepancy can be explained by differences in the $B_{A_1^\square A_1^\circ}^E$ and B_{33}^E elastic constants. This can be verified at $T = 300$ K by taking the experimental values of $e_{\alpha i}$ and B_{ij} from Ref. [68] and replacing the values of $B_{A_1^\square A_1^\circ}^E$ and B_{33}^E with our computed values of 108.1 GPa and 56.0 GPa which yields $d_{31} = -39.9$ pC/N, in good agreement with our pure gQHA result (additional replacements did not have an appreciable effect). The temperature dependence of d_{31} within the gQHA is in good agreement with experimental measurements up to room temperature [71], though the agreement is likely fortuitous given the discrepancies in the temperature dependence of the elastic constants, thermal expansion, and the relaxed-ion piezoelectric stress coefficients. Therefore, the anomalous temperature dependence of d_{31} beyond room temperature is not entirely unanticipated.

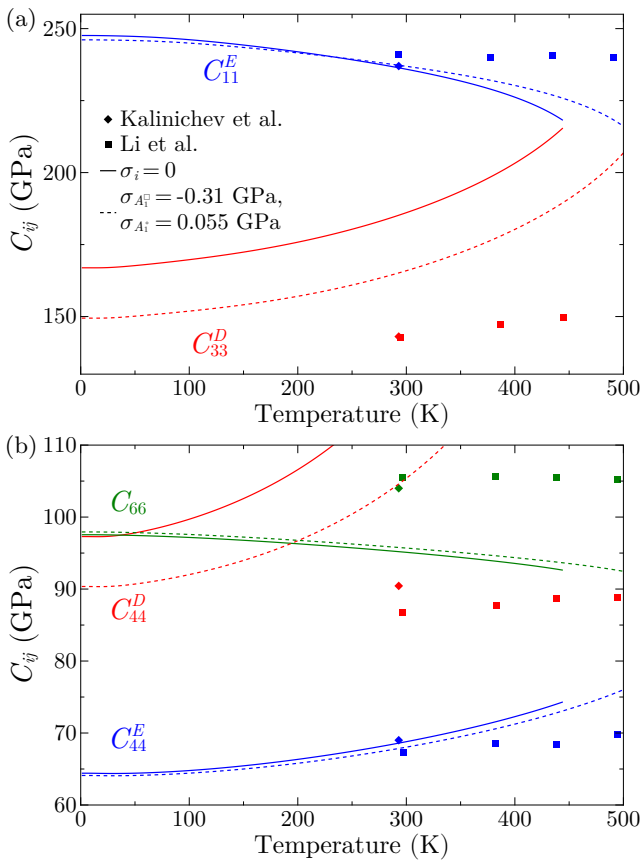


FIG. 3. Selected axial (a) and shear (b) elastic constants under constant E fields or D fields computed with the gQHA (lines) under unstressed (solid) and stressed (dashed) conditions compared with previous experimental measurements (markers) [68, 69]. See SM for additional elastic constants [40].

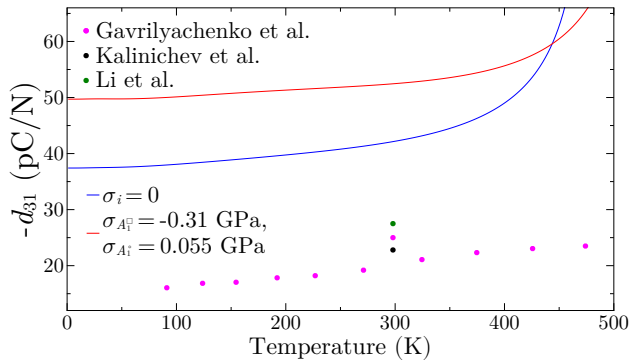


FIG. 4. Piezoelectric strain coefficient $-d_{31}$ computed with gQHA (lines) under unstressed (blue) and stressed (red) conditions compared with existing experimental measurements (circles) [68, 69, 71]. For additional piezoelectric strain coefficients, see SM [40].

In summary, we have demonstrated the application of the gQHA to a non-cubic crystal, ferroelectric $PbTiO_3$, under conditions of finite temperature and stress. The irreducible derivative approach to computing phonons from finite difference yields the strain dependent phonons, where dipole-quadrupole effects are incorporated in the Fourier interpolation. The thermal expansion, elastic constants, and piezoelectric strain coefficients are computed at finite temperature and stress. The temperature dependence of the thermal expansion and elastic constants at zero stress are over estimated by the gQHA, illustrating the need to solve the vibrational Hamiltonian using a strain-dependent theory which explicitly accounts for phonon interactions. Our observed limitations of the gQHA are not unexpected, as discrepancies of the QHA are well known in various anharmonic materials [57, 58]. Advances in the computation of finite temperature vibrational properties from DFT using more sophisticated approximations than the QHA have been achieved [72–77], however we are not aware of the application of any of these theories to the computation of the elastic constant tensor at finite temperature. These more advanced theories can be straightforwardly applied as a function of strain to compute thermal expansion and elastic constants at finite temperature and stress using the general formalism outlined previously [26], which will be the subject of future work.

This work was supported by the grant DE-SC0016507 funded by the U.S. Department of Energy, Office of Science. This research used resources of the National Energy Research Scientific Computing Center, a DOE Office of Science User Facility supported by the Office of Science of the U.S. Department of Energy under Contract No. DE-AC02-05CH11231.

[1] M. E. Lines and A. M. Glass, *Principles and Applications of Ferroelectrics and Related Materials* (Oxford University Press, 2001).
[2] N. Setter, D. Damjanovic, L. Eng, G. Fox, S. Gevorgian, S. Hong, A. Kingon, H. Kohlstedt, N. Park, G. Stephenson, *et al.*, Ferroelectric thin films: Review of materials, properties, and applications, Journal of Applied Physics **100**, 051606 (2006).
[3] K. M. Rabe, C. H. Ahn, and J.-M. Triscone, *Physics of ferroelectrics: a modern perspective*, Vol. 105 (Springer Science & Business Media, 2007).
[4] R. E. Cohen, First-principles theories of piezoelectric materials, in *Piezoelectricity: Evolution and Future of a Technology*, Springer Series in Materials Science, edited by W. Heywang, K. Lubitz, and W. Wersing (Springer, Berlin, Heidelberg, 2008) p. 471–492.
[5] H. Liu, J. Zhong, C. Lee, S.-W. Lee, and L. Lin, A comprehensive review on piezoelectric energy harvesting technology: Materials, mechanisms, and applications, Applied Physics Reviews **5**, 041306 (2018).
[6] W. Zhong, D. Vanderbilt, and K. M. Rabe, First-principles theory of ferroelectric phase transitions for perovskites: The case of batio$_3$, Phys. Rev. B **52**, 6301 (1995).
[7] K. M. Rabe and U. V. Waghmare, Strain Coupling in the PbTiO3 Ferroelectric Transition on JSTOR, Philosophical Transactions: Mathematical, Physical and Engineering Sciences **354**, 2897 (1996).
[8] U. V. Waghmare and K. M. Rabe, Ab initio statistical mechanics of the ferroelectric phase transition in $PbTiO_3$, Physical Review B **55**, 6161 (1997).
[9] J. C. Wojdeł, P. Hermet, M. P. Ljungberg, P. Ghosez, and J. Íñiguez, First-principles model potentials for lattice-dynamical studies: general methodology and example of application to ferroic perovskite oxides, Journal of Physics: Condensed Matter **25**, 305401 (2013).
[10] A. Togo, L. Chaput, I. Tanaka, and G. Hug, First-principles phonon calculations of thermal expansion in Ti_3SiC_2, Ti_3AlC_2, and Ti_3GeC_2, Physical Review B **81**, 174301 (2010).
[11] R. M. Wentzcovitch, Z. Q. Wu, and P. Carrier, First principles quasiharmonic thermoelasticity of mantle minerals, Theoretical And Computational Methods In Mineral Physics: Geophysical Applications Se Reviews In Mineralogy & Geochemistry **71**, 99 (2010).
[12] S. Baroni, P. Giannozzi, and E. Isaev, Density-functional perturbation theory for quasi-harmonic calculations, Theoretical And Computational Methods In Mineral Physics: Geophysical Applications Se Reviews In Mineralogy & Geochemistry **71**, 39 (2010).
[13] R. Masuki, T. Nomoto, R. Arita, and T. Tadano, Full optimization of quasiharmonic free energy with an anharmonic lattice model: Application to thermal expansion and pyroelectricity of wurtzite gan and zno, Phys. Rev. B **107**, 134119 (2023).
[14] B. B. Karki, R. M. Wentzcovitch, S. de Gironcoli, and S. Baroni, High-pressure lattice dynamics and thermoelasticity of mgo, Phys. Rev. B **61**, 8793 (2000).
[15] G. J. Ackland, X. Huang, and K. M. Rabe, First-principles thermodynamics of transition metals: W, NiAl, and PdTi, Physical Review B **68**, 214104 (2003).
[16] X. Sha and R. E. Cohen, First-principles thermoelasticity of bcc iron under pressure, Physical Review B **74**, 214111 (2006).
[17] H. H. Pham, M. E. Williams, P. Mahaffey, M. Radovic, R. Arroyave, and T. Cagin, Finite-temperature elasticity of fcc Al: Atomistic simulations and ultrasonic measurements, Physical Review B **84**, 064101 (2011).
[18] D. Dragoni, D. Ceresoli, and N. Marzari, Thermoelastic properties of α-iron from first-principles, Physical Review B **91**, 104105 (2015).
[19] L.-F. Huang, X.-Z. Lu, E. Tennessen, and J. M. Rondinelli, An efficient ab-initio quasiharmonic approach for the thermodynamics of solids, Computational Materials Science **120**, 84 (2016).
[20] C. Malica and A. D. corso, Quasi-harmonic temperature dependent elastic constants: applications to silicon, aluminum, and silver, Journal Of Physics-condensed Matter **32**, 315902 (2020).
[21] C. Malica and A. Dal Corso, Quasi-harmonic thermoelasticity of palladium, platinum, copper, and gold from first principles, Journal of Physics: Condensed Matter

33, 475901 (2021).
[22] .
[23] T. Shao, B. Wen, R. Melnik, S. Yao, Y. Kawazoe, and Y. Tian, Temperature dependent elastic constants for crystals with arbitrary symmetry: Combined first principles and continuum elasticity theory, Journal of Applied Physics **111**, 083525 (2012).
[24] A. Bakare and A. Bongiorno, Enhancing efficiency and scope of first-principles quasiharmonic approximation methods through the calculation of third-order elastic constants, Physical Review Materials **6**, 043803 (2022).
[25] P. A. Olsson, Ab initio thermo-elasticity of δ-mhx (m= zr, ti), Computational Materials Science **218**, 111953 (2023).
[26] M. A. Mathis, A. Khanolkar, L. Fu, M. S. Bryan, C. A. Dennett, K. Rickert, J. M. Mann, B. Winn, D. L. Abernathy, M. E. Manley, D. H. Hurley, and C. A. Marianetti, Generalized quasiharmonic approximation via space group irreducible derivatives, Phys. Rev. B **106**, 014314 (2022).
[27] L. Fu, M. Kornbluth, Z. Cheng, and C. A. Marianetti, Group theoretical approach to computing phonons and their interactions, Phys. Rev. B **100**, 014303 (2019).
[28] S. Bandi and C. A. Marianetti, Precisely computing phonons via irreducible derivatives, Physical Review B **107**, 174302 (2023).
[29] G. Shirane and S. Hoshino, On the Phase Transition in Lead Titanate, Journal of the Physical Society of Japan **6**, 265 (1951).
[30] J. Zhu, H. Xu, J. Zhang, C. Jin, L. Wang, and Y. Zhao, Thermal equations of state and phase relation of PbTiO3: A high P-T synchrotron x-ray diffraction study, Journal of Applied Physics **110**, 10.1063/1.3651377 (2011).
[31] S. G. Jabarov, D. P. Kozlenko, S. E. Kichanov, A. V. Belushkin, B. N. Savenko, R. Z. Mextieva, and C. Lathe, High-pressure effect on the ferroelectric-paraelectric transition in PbTiO3, Physics of the Solid State **53**, 2300 (2011).
[32] G. Kresse and J. Hafner, Abinitio molecular-dynamics for liquid-metals, Phys. Rev. B **47**, 558 (1993).
[33] G. Kresse and J. Hafner, Ab-initio molecular-dynamics simulation of the liquid-metal amorphous-semiconductor transition in germanium, Phys. Rev. B **49**, 14251 (1994).
[34] G. Kresse and J. Furthmuller, Efficiency of ab-initio total energy calculations for metals and semiconductors using a plane-wave basis set, Computational Materials Science **6**, 15 (1996).
[35] G. Kresse and J. Furthmuller, Efficient iterative schemes for ab initio total-energy calculations using a plane-wave basis set, Phys. Rev. B **54**, 11169 (1996).
[36] P. E. Blochl, Projector augmented-wave method, Phys. Rev. B **50**, 17953 (1994).
[37] G. Kresse and D. Joubert, From ultrasoft pseudopotentials to the projector augmented-wave method, Phys. Rev. B **59**, 1758 (1999).
[38] J. P. Perdew, A. Ruzsinszky, G. I. Csonka, O. A. Vydrov, G. E. Scuseria, L. A. Constantin, X. Zhou, and K. Burke, Restoring the density-gradient expansion for exchange in solids and surfaces, Physical Review Letters **100**, 136406 (2008).
[39] J. W. Sun, A. Ruzsinszky, and J. P. Perdew, Strongly constrained and appropriately normed semilocal density functional, Phys. Rev. Lett. **115**, 036402 (2015).
[40] See Supplemental Material at [link] for additional computational details, additional elastic constant computations, and additional piezoelectric strain coefficient computations. Refs. [68, 78, 79] were cited.
[41] H. Meštrić, R.-A. Eichel, T. Kloss, K.-P. Dinse, S. Laubach, S. Laubach, P. C. Schmidt, K. A. Schönau, M. Knapp, and H. Ehrenberg, Iron-oxygen vacancy defect centers in $PbTio_3$: Newman superposition model analysis and density functional calculations, Phys. Rev. B **71**, 134109 (2005).
[42] E. T. Ritz and N. A. Benedek, Interplay between Phonons and Anisotropic Elasticity Drives Negative Thermal Expansion in $PbTiO_3$, Physical Review Letters **121**, 255901 (2018).
[43] P. Giannozzi, S. de Gironcoli, P. Pavone, and S. Baroni, Abinitio calculation of phonon dispersions in semiconductors, Phys. Rev. B **43**, 7231 (1991).
[44] X. Gonze and C. Lee, Dynamical matrices, born effective charges, dielectric permittivity tensors, and interatomic force constants from density-functional perturbation theory, Phys. Rev. B **55**, 10355 (1997).
[45] S. Baroni, S. de Gironcoli, A. DalCorso, and P. Giannozzi, Phonons and related crystal properties from density-functional perturbation theory, Rev. Mod. Phys. **73**, 515 (2001).
[46] M. Gajdos, K. Hummer, G. Kresse, J. Furthmuller, and F. Bechstedt, Linear optical properties in the projector-augmented wave methodology, Phys. Rev. B **73**, 045112 (2006).
[47] M. Royo, K. R. Hahn, and M. Stengel, Using high multipolar orders to reconstruct the sound velocity in piezoelectrics from lattice dynamics, Physical Review Letters **125**, 217602 (2020).
[48] M. Royo and M. Stengel, First-principles theory of spatial dispersion: Dynamical quadrupoles and flexoelectricity, Physical Review X **9**, 021050 (2019).
[49] X. Gonze, B. Amadon, G. Antonius, F. Arnardi, L. Baguet, J.-M. Beuken, J. Bieder, F. Bottin, J. Bouchet, E. Bousquet, N. Brouwer, F. Bruneval, G. Brunin, T. Cavignac, J.-B. Charraud, W. Chen, M. Côté, S. Cottenier, J. Denier, G. Geneste, P. Ghosez, M. Giantomassi, Y. Gillet, O. Gingras, D. R. Hamann, G. Hautier, X. He, N. Helbig, N. Holzwarth, Y. Jia, F. Jollet, W. Lafargue-Dit-Hauret, K. Lejaeghere, M. A. L. Marques, A. Martin, C. Martins, H. P. C. Miranda, F. Naccarato, K. Persson, G. Petretto, V. Planes, Y. Pouillon, S. Prokhorenko, F. Ricci, G.-M. Rignanese, A. H. Romero, M. M. Schmitt, M. Torrent, M. J. van Setten, B. V. Troeye, M. J. Verstraete, G. Zérah, and J. W. Zwanziger, The abinit project: Impact, environment and recent developments, Comput. Phys. Commun. **248**, 107042 (2020).
[50] A. H. Romero, D. C. Allan, B. Amadon, G. Antonius, T. Applencourt, L. Baguet, J. Bieder, F. Bottin, J. Bouchet, E. Bousquet, F. Bruneval, G. Brunin, D. Caliste, M. Côté, J. Denier, C. Dreyer, P. Ghosez, M. Giantomassi, Y. Gillet, O. Gingras, D. R. Hamann, G. Hautier, F. Jollet, G. Jomard, A. Martin, H. P. C. Miranda, F. Naccarato, G. Petretto, N. A. Pike, V. Planes, S. Prokhorenko, T. Rangel, F. Ricci, G.-M. Rignanese, M. Royo, M. Stengel, M. Torrent, M. J. van Setten, B. V. Troeye, M. J. Verstraete, J. Wiktor, J. W. Zwanziger, and X. Gonze, Abinit: Overview, and focus on selected capabilities, J. Chem. Phys. **152**, 124102 (2020).
[51] D. R. Hamann, Optimized norm-conserving vanderbilt

pseudopotentials, Phys. Rev. B **88**, 085117 (2013).
[52] N. L. Allan, T. H. K. Barron, and J. A. O. Bruno, The zero static internal stress approximation in lattice dynamics, and the calculation of isotope effects on molar volumes, The Journal of Chemical Physics **105**, 8300 (1996).
[53] J. Liu, M. V. Fernández-Serra, and P. B. Allen, First-principles study of pyroelectricity in gan and zno, Phys. Rev. B **93**, 081205 (2016).
[54] J. Liu and S. T. Pantelides, Mechanisms of pyroelectricity in three- and two-dimensional materials, Phys. Rev. Lett. **120**, 207602 (2018).
[55] J. Liu and P. B. Allen, Internal and external thermal expansions of wurtzite zno from first principles, Computational Materials Science **154**, 251 (2018).
[56] J. Chen, X. R. Xing, R. B. Yu, and G. R. Liu, Structure and enhancement of negative thermal expansion in the PbTiO3–CdTiO3 system, Applied Physics Letters **87**, 231915 (2005).
[57] P. B. Allen, Anharmonic phonon quasiparticle theory of zero-point and thermal shifts in insulators: heat capacity, bulk modulus, and thermal expansion, Phys. Rev. B **92**, 064106 (2015).
[58] R. Masuki, T. Nomoto, R. Arita, and T. Tadano, Anharmonic grüneisen theory based on self-consistent phonon theory: Impact of phonon-phonon interactions neglected in the quasiharmonic theory, Physical Review B **105**, 064112 (2022).
[59] J. Kobayashi, Y. Uesu, and Y. Sakemi, X-ray and optical studies on phase transition of $PbTiO_3$ at low temperatures, Physical Review B **28**, 3866 (1983).
[60] C. Sun, Z. Cao, J. Chen, R. Yu, X. Sun, P. Hu, G. Liu, and X. Xing, Negative thermal expansion in the pbti1–x fex o3 system, physica status solidi (b) **245**, 2520 (2008).
[61] A. Sani, M. Hanfland, and D. Levy, Pressure and temperature dependence of the ferroelectric–paraelectric phase transition in pbtio3, Journal of Solid State Chemistry **167**, 446–452 (2002).
[62] D. Wallace, *Thermodynamics of Crystals* (Dover, 1998).
[63] X. Wu, D. Vanderbilt, and D. R. Hamann, Systematic treatment of displacements, strains, and electric fields in density-functional perturbation theory, Phys. Rev. B **72**, 035105 (2005).
[64] S. de Gironcoli, S. Baroni, and R. Resta, Piezoelectric properties of III-V semiconductors from first-principles linear-response theory, Physical Review Letters **62**, 2853 (1989).
[65] G. Sághi-Szabó, R. E. Cohen, and H. Krakauer, First-principles study of piezoelectricity in $pbtio_3$, Phys. Rev. Lett. **80**, 4321 (1998).
[66] G. Sághi-Szabó, R. E. Cohen, and H. Krakauer, First-principles study of piezoelectricity in tetragonal $pbtio_3$ and $pbzr_{1/2}ti_{1/2}o_3$, Phys. Rev. B **59**, 12771 (1999).
[67] Z. Li, M. Grimsditch, X. Xu, and S. K. Chan, The elastic, piezoelectric and dielectric constants of tetragonal pbtio3 single crystals, Ferroelectrics **141**, 313–325 (1993).
[68] A. G. Kalinichev, J. D. Bass, B. N. Sun, and D. A. Payne, Elastic properties of tetragonal pbtio 3 single crystals by brillouin scattering, Journal of Materials Research **12**, 2623–2627 (1997).
[69] Z. Li, M. Grimsditch, C. M. Foster, and S. K. Chan, Dielectric and elastic properties of ferroelectric materials at elevated temperature, Journal of Physics and Chemistry of Solids Proceeding of the 3rd Williamsburg Workshop on Fundamental Experiments on Ferroelectrics, **57**, 1433–1438 (1996).
[70] J. F. Nye, *Physical properties of crystals: their representation by tensors and matrices* (Oxford university press, 1985).
[71] V. Gavrilyachenko and E. Fesenko, Piezoelectric effect in lead titanate single crystals (1971).
[72] P. Souvatzis, O. Eriksson, M. I. Katsnelson, and S. P. Rudin, Entropy Driven Stabilization of Energetically Unstable Crystal Structures Explained from First Principles Theory, Physical Review Letters **100**, 095901 (2008).
[73] P. Souvatzis, O. Eriksson, M. I. Katsnelson, and S. P. Rudin, The self-consistent ab initio lattice dynamical method, Computational Materials Science **44**, 888 (2009).
[74] O. Hellman, I. A. Abrikosov, and S. I. Simak, Lattice dynamics of anharmonic solids from first principles, Physical Review B **84**, 180301 (2011).
[75] I. Errea, M. Calandra, and F. Mauri, Anharmonic free energies and phonon dispersions from the stochastic self-consistent harmonic approximation: Application to platinum and palladium hydrides, Physical Review B **89**, 064302 (2014).
[76] T. Tadano and S. Tsuneyuki, Self-consistent phonon calculations of lattice dynamical properties in cubic $SrTiO_3$ with first-principles anharmonic force constants, Physical Review B **92**, 054301 (2015).
[77] E. Xiao and C. A. Marianetti, Anharmonic phonon behavior via irreducible derivatives: Self-consistent perturbation theory and molecular dynamics, Physical Review B **107**, 094303 (2023).
[78] P. E. Blochl, O. Jepsen, and O. K. Andersen, Improved tetrahedron method for brillouin-zone integrations, Phys. Rev. B **49**, 16223 (1994).
[79] A. Paul, J. Sun, J. P. Perdew, and U. V. Waghmare, Accuracy of first-principles interatomic interactions and predictions of ferroelectric phase transitions in perovskite oxides: Energy functional and effective Hamiltonian, Physical Review B **95**, 054111 (2017).